# Time-Dependent Block and Resurgent Tail Currents Induced by Mouse $\beta4_{154–167}$ Peptide in Cardiac $Na^+$ Channels

Ging Kuo Wang,[1] Thomas Edrich,[1] and Sho-Ya Wang[2]

[1]Department of Anesthesia, Harvard Medical School and Brigham and Women's Hospital, Boston, MA 02115
[2]Department of Biology, State University of New York at Albany, Albany, NY 12222

Resurgent tail $Na^+$ currents were first discovered in cerebellar Purkinje neurons. A recent study showed that a 14-mer fragment of a mouse β4 subunit, $\beta4_{154–167}$, acts as an intracellular open-channel blocker and elicits resurgent currents in Purkinje neurons (Grieco, T.M., J.D. Malhotra, C. Chen, L.L. Isom, and I.M. Raman. 2005. *Neuron.* 45:233–244). To explore these phenotypes in vitro, we characterized $\beta4_{154–167}$ actions in inactivation-deficient cardiac hNav1.5 $Na^+$ channels expressed in human embryonic kidney 293t cells. Intracellular $\beta4_{154–167}$ from 25–250 μM elicited a conspicuous time-dependent block of inactivation-deficient $Na^+$ currents at 50 mV in a concentration-dependent manner. On and off rates for $\beta4_{154–167}$ binding were estimated at 10.1 $\mu M^{-1}s^{-1}$ and 49.1 $s^{-1}$, respectively. Upon repolarization, large tail currents emerged with a slight delay at −140 mV, probably as a result of the rapid unblocking of $\beta4_{154–167}$. Near the activation threshold (approximately −70 mV), resurgent tail currents were robust and long lasting. Likewise, $\beta4_{154–167}$ induces resurgent currents in wild-type hNav1.5 $Na^+$ channels, although to a lesser extent. The inactivation peptide acetyl-KIFMK-amide not only restored the fast inactivation phenotype in hNav1.5 inactivation-deficient $Na^+$ channels but also elicited robust resurgent currents. When modified by batrachotoxin (BTX), wild-type hNav1.5 $Na^+$ channels opened persistently but became resistant to $\beta4_{154–167}$ and acetyl-KIFMK-amide block. Finally, a lysine substitution of a phenylalanine residue at D4S6, F1760, which forms a part of receptors for local anesthetics and BTX, rendered cardiac $Na^+$ channels resistant to $\beta4_{154–167}$. Together, our in vitro studies identify a putative S6-binding site for $\beta4_{154–167}$ within the inner cavity of hNav1.5 $Na^+$ channels. Such an S6 receptor readily explains (1) why $\beta4_{154–167}$ gains access to its receptor as an open-channel blocker, (2), why bound $\beta4_{154–167}$ briefly prevents the activation gate from closing by a "foot-in-the-door" mechanism during deactivation, (3) why BTX inhibits $\beta4_{154–167}$ binding by physical exclusion, and (4) why a lysine substitution of residue F1760 eliminates $\beta4_{154–167}$ binding.

The Journal of General Physiology

## INTRODUCTION

Mammalian voltage-gated $Na^+$ channels are responsible for the generation of action potentials in excitable membranes. These channels consist of one large α subunit along with one or two small auxiliary β subunits (Catterall, 2000). Nine α subunits (Nav1.1–1.9) and four β subunits (β1–4) have been identified to date. When expressed in human embryonic kidney 293 (HEK293) cells, the α subunit alone forms a functional channel, which appears comparable with the native $Na^+$ channel (Ukomadu et al., 1992).

Voltage-gated $Na^+$ channels are activated by depolarization and, once open, are quickly inactivated through the action of an inactivation particle, which rapidly blocks the open pore (Armstrong and Benzanilla, 1977). Armstrong (1981) proposed a "foot-in-the-door" model for fast inactivation. His model states that (1) an inactivating particle can block the channel only if the activation gate is open and that (2) closing of the activation gate is hindered by a foot-in-the-door effect once the inactivation particle is in the channel mouth. Because $Na^+$ channels do not leak during recovery from inactivation, the foot-in-the-door model also requires that the activation gate (door) is partially closed before the withdrawal of the inactivation particle (foot). The partially deactivated $Na^+$ channel does not conduct while the inactivation particle is withdrawn from the pore. The inactivation particle likely contains an IFM motif located within the intracellular D3-D4 linker of the $Na^+$ channel α subunit as deduced by site-directed mutagenesis (West et al., 1992). A synthetic peptide, acetyl-KIFMK-amide, can restore fast inactivation in inactivation-deficient rNav1.2 and hNav1.5 $Na^+$ channels (Eaholtz et al., 1994; Tang et al., 1996; Wang and Wang, 2005).

In the cerebellum, Purkinje neurons often fire high-frequency action potentials with a rate near 100 Hz. Such rapid discharges require short refractory periods. Earlier classical studies indicated that Purkinje $Na^+$ channels may be subject to a rapid, voltage-dependent open-channel block by an unknown endogenous blocker (Raman and Bean, 1997; Raman et al., 1997). By blocking the pore during depolarization and rapid unblocking upon

Correspondence to Ging Kuo Wang: wang@zeus.bwh.harvard.edu

Abbreviations used in this paper: BTX, batrachotoxin; HEK, human embryonic kidney.

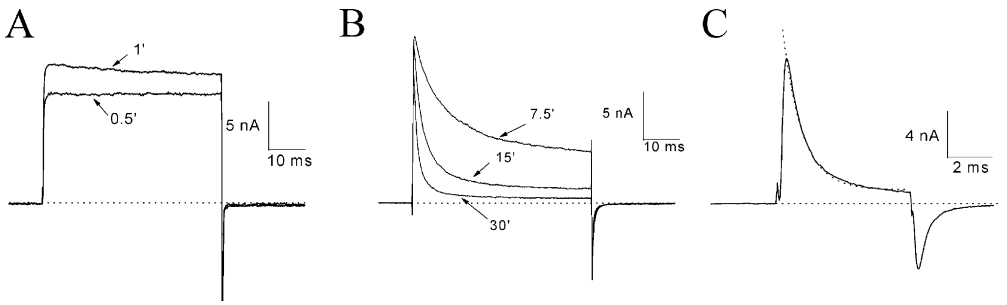


**Figure 1.** Time-dependent block induced by $\beta4_{154–167}$ at 50 mV. Current traces of hNav1.5-CW mutant channels were recorded after the pipette break-in under the whole-cell configuration. The pipette solution contained 125 μM $\beta4_{154–167}$. (A) Currents became larger during initial dialysis but exhibited little or no fast inactivation. Traces were recorded at the times labeled. (B) The time-dependent block was progressively developed during continued dialysis and reached steady state around 15–30 minutes. (C) The time-dependent block was well fitted by a single exponential function with a τ value of 0.86 ms (dashed line). Holding potential was set at −140 mV.

repolarization, this endogenous blocker prevents the conventional fast inactivation particle from binding, thereby accelerating recovery. While the blocker is expelled from the pore, a brief resurgent $Na^+$ current emerges upon repolarization. This resurgent tail $Na^+$ current could account for the high frequency firings in Purkinje neurons (Raman and Bean, 2001). More recently, Grieco et al. (2005) reported that $\beta4_{154–167}$, the cytoplasmic tail of the mouse β4 subunit (KKLITFILKKTREK), blocked $Na^+$ channels and elicited resurgent $Na^+$ currents in Purkinje neurons. These authors proposed that the β4 cytoplasmic tail is the endogenous open-channel blocker responsible for resurgent kinetics. The major $Na^+$ channel isoform in cerebellar Purkinje neurons is the Nav1.6. However, resurgent $Na^+$ current is not completely abolished in Nav1.6-null Purkinje neurons (Grieco and Raman, 2004), indicating that the resurgent $Na^+$ current may not be limited to neuronal Nav1.6.

The β4 subunit has been detected in cardiac tissues (Yu et al., 2003; Maier et al., 2004), but its role in the heart remains unknown. Most, if not all, studies concerning resurgent currents have used neurons from the central nervous system or dorsal root ganglion (Do and Bean, 2004; Grieco and Raman, 2004; Cummins et al., 2005). In this study, we asked whether mouse $\beta4_{154–167}$ acts as an open-channel blocker in cardiac hNav1.5 channels. We addressed this question primarily using inactivation-deficient mutant hNav1.5-L409C/A410W $Na^+$ channels (hNav1.5-CW) expressed in HEK293t cells. In this mutant channel, the native D1S6 residues leucine (L) at position 409 and alanine (A) at position 410 were replaced by cysteine (C) and tryptophan (W), respectively. This D1S6 region is not directly involved in acetyl-KIFMK-amide binding, although mutations at this site may prevent access of the intrinsic fast inactivation particle to the inner cavity (Wang and Wang, 2005). The HEK expression system allowed us to characterize pharmacological actions of $\beta4_{154–167}$ and to define the $\beta4_{154–167}$ receptor in the hNav1.5 channel by site-directed mutagenesis. Our results suggest that $\beta4_{154–167}$ binds near the activation gate within the inner cavity and briefly prevents the gate from closing, which is analogous to the foot-in-the-door mechanism proposed by Armstrong (1981).

## MATERIALS AND METHODS

### Site-Directed Mutagenesis

We used the QuikChange XL Site-Directed Mutagenesis Kit (Stratagene) to create an inactivation-deficient hNav1.5-CW mutant clone within the pcDNA1/Amp vector (Wang et al., 2003; Wang and Wang, 2005). An additional mutation, hNav1.5-CW/F1760K, was derived using the same method. Other inactivation-deficient mutants, rNav1.4-L435W/L437C/A438W (rNav1.4-WCW) and rNav1.4-WCW/F1579K (Wang et al., 2003), were also created.

### Transient Transfection

HEK293t cells were grown to ∼50% confluence in Dulbecco's modified Eagle's medium (Life Technologies) containing 10% FBS (HyClone), 1% penicillin and streptomycin solution (Sigma-Aldrich), 3 mM taurine, and 25 mM HEPES (Life Technologies) and were transfected by calcium phosphate precipitation. Transfection of 5–10 μg of wild-type hNav1.5-CW along with 10–20 μg of rat β1-pcDNA1/Amp and 1 μg of reporter CD8-pih3m was adequate for current recording. Rat β1 subunit was included to increase the level of the channel expression. Cells were replated 15 h after transfection in 35-mm dishes, maintained at 37°C in a 5% $CO_2$ incubator, and used after 1–4 d. Transfection-positive cells were identified with immunobeads (CD8-Dynabeads; Invitrogen).

### Whole-Cell Voltage Clamp

Whole-cell configuration was used to record $Na^+$ current (Hamill et al., 1981). Borosilicate micropipettes were pulled (P-87; Sutter Instrument Co.) and heat polished. Pipette electrodes contained 100 mM NaF, 30 mM NaCl, 10 mM EGTA, and 10 mM HEPES adjusted to pH 7.2 with CsOH. The pipette electrodes had a tip resistance of 0.5–1.0 MΩ. Access resistance was generally 1–2 MΩ. We minimized the series resistance (>85%) and corrected the leak and capacitance using a patch clamp amplifier (Axopatch 200B; Molecular Devices). Holding potential was set at −140 mV. Further correction was achieved by P/−4 protocol. The tail current was normally recorded at a rate of 20–40 μs per point. It is noteworthy that the accuracy of the rising phase of the tail current records is dependent on the speed of the Axopatch amplifier. It could take ∼170 μs to reach 80% of the final voltage applied (Cota and Armstrong, 1989). With supercharging compensation by Axopatch, the tail currents appeared to reach their peak amplitude more rapidly. Unfortunately, a large spike was introduced by this device and prevented us from using such correction. To verify that the differences existed in tail

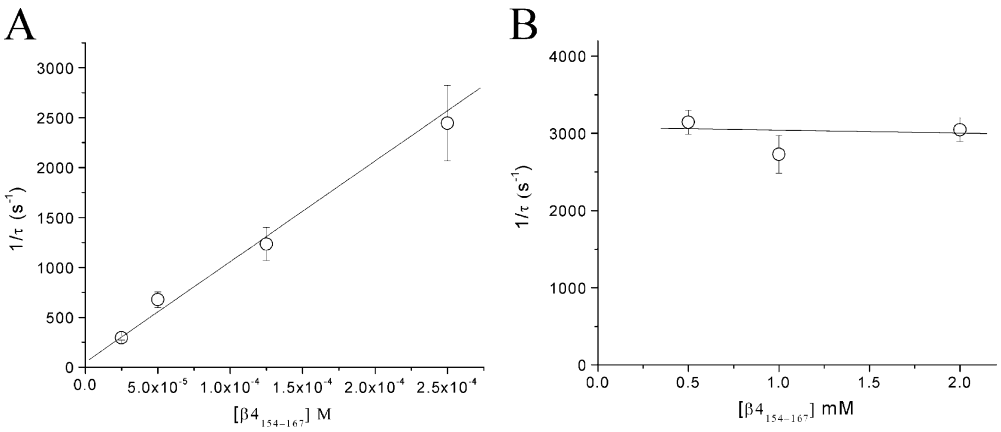


**Figure 2.** On and off rates of $\beta4_{154–167}$ binding at 50 mV. (A) The τ values were recorded ininactivation-deficient hNav1.5-CW mutant channels at $\beta4_{154–167}$ concentrations ranging from 25 to 250 μM, inverted, and plotted against the corresponding concentration ($n$ = 5). The plot was fitted by a linear regression to yield y = 49.1 + (10.1 × $10^6$) × x. Off rate ($k_1$ = x intercept) was estimated to be 49.1 $s^{-1}$, and the on rate ($k_1$ = slope) was 10.1 $[\mu M]^{-1}s^{-1}$. (B) The τ values were recorded at $\beta4_{154–167}$ concentrations rang-ing from 0.5 to 2 mM, inverted, and plotted against the corresponding concentration. The τ values did not vary significantly at this concentration range ($P > 0.05$; $n$ = 6). Error bars represent SEM.

currents with and without the peptide, we superimposed the tail currents for direct comparison and included the measurement of the area under the tail currents (nano-amperes × milliseconds).

Experiments were performed at room temperature (22–24°C) under a $Na^+$-containing bath solution with 65 mM NaCl, 85 mM choline Cl, 2 mM $CaCl_2$, and 10 mM HEPES adjusted to pH 7.4 with tetramethylammonium hydroxide. In a few cases, we exchanged NaCl with choline Cl with a final external $Na^+$ concentration of 0 or 130 mM. An unpaired $t$ test was used to evaluate estimated parameters (mean ± SEM or fitted value ± SEM of the fit); P values of $< 0.05$ were considered statistically significant.

### Drug Solutions

Peptide $\beta4_{154–167}$ with a mouse β4 sequence (KKLITFILKKTREK) was synthesized by Biopeptide Co. (>95% pure), dissolved in the pipette solution at a 5-mM stock concentration, aliquoted, and stored at −20°C. The final peptide solution was prepared, stored at −20°C, and thawed. We used a 1-ml syringe to withdraw an appropriate amount of the final peptide solution and kept it at 4°C. Under these conditions, we observed no changes in $\beta4_{154–167}$ activity. Under whole-cell configuration, HEK293t cells survived routinely for >1 h, which is long enough for the peptide block to reach its steady state even at low concentrations. Acetyl-KIFMK-amide was synthesized, dissolved at a 10-mM stock concentration, and prepared as described previously (Wang and Wang, 2005). Batrachotoxin (BTX) was provided by J. Daly (National Institutes of Health, Bethesda, MD) and was dissolved in DMSO at 0.5 mM. The final concentration of BTX was 4 μM.

### Computer Simulation

For $\beta4_{154–167}$ block, we used a simplified gating model from Raman and Bean (2001) without the fast inactivation particle.

(SCHEME 1)

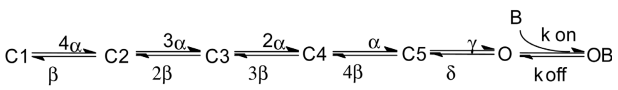


This is a statistical model in which channels must transition through five sequential closed states (C1–C5) before reaching the open state (O), which allows $Na^+$ ions to flow through. First-order kinetics describe these transitions using the voltage-dependent coefficients α, β, γ, and δ (in $seconds^{-1}$), which are: $\alpha = 1.6\ e^{V/40}$, $\beta = 0.3\ e^{-V/40}$, $\gamma = 50\ e^{V/100}$, and $\delta = 0.6\ e^{-V/25}$, where V is in millivolts. These coefficients were obtained by repetitive approximation to minimize the mean square error between the experimental data and the simulated current traces. The open channel is blocked by peptide $\beta4_{154–167}$ (B) as governed by $k_{on}$ ($Molar^{-1}$ × $seconds^{-1}$) and $k_{off}$ ($seconds^{-1}$).

## RESULTS

### Block of Inactivation-Deficient Mutant $Na^+$ Currents by Internal $\beta4_{154–167}$

We investigated the effects of $\beta4_{154–167}$ first in inactivation-deficient hNav1.5-L409C/A410W mutant $Na^+$ channels at 50 mV where fast inactivation was minimal or absent (Fig. 1 A). After the pipette break-in, the outward current became larger initially as the pipette solution contained a high $[Na^+]_{in}$ (65 mM). Within a few minutes, the $Na^+$ currents reached a quasi steady-state level, and, from then on, $\beta4_{154–167}$ began to block the maintained $Na^+$ currents as if $\beta4_{154–167}$ restored the fast inactivation phenotype (Fig. 1 B). With 125 μM $\beta4_{154–167}$ in the pipette, this time-dependent blocking phenotype reached its steady state by ∼15–30 min. At steady state, the current decay was well fitted by a single exponential function with a time constant (τ) of 0.84 ± 0.18 ms ($n$ = 5; Fig. 1 C, dashed line). Such a time-dependent block phenotype was detected in dissociated neurons with the help of a wasp toxin, β-pompilidotoxin, which slowed the fast inactivation gating considerably (Grieco and Raman, 2004). In contrast, without peptide present, most hNav1.5-CW $Na^+$ currents were noninactivating at 50 mV (Fig. 1 A; Wang and Wang, 2005).

### On and Off Rates of $\beta4_{154–167}$ Binding in Inactivation-Deficient $Na^+$ Channels

To determine the on and off rates of $\beta4_{154–167}$ block, we measured the τ values at various peptide concentrations ranging from 25 to 250 μM as described in Fig. 1 C. The τ values were inverted and plotted against the

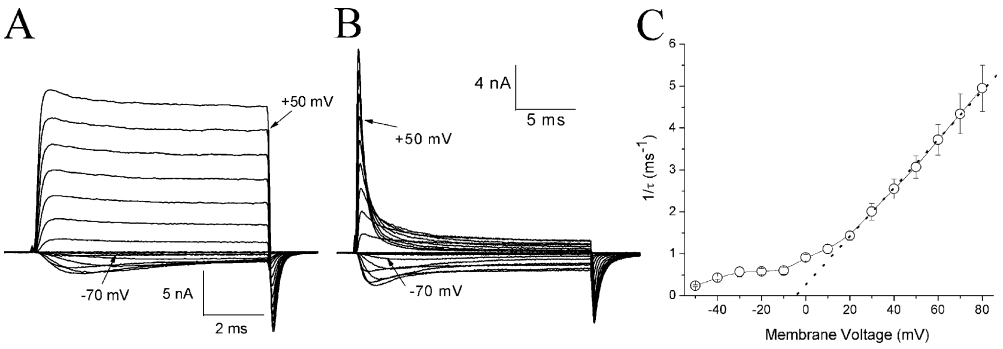


**Figure 3.** Time-dependent block at various voltages. Families of superimposed hNav1.5-CW current traces were recorded at various voltages in the absence (A) and presence (B) of 125 μM $\beta4_{154–167}$. Traces corresponding to −70 and 50 mV are labeled. For the steady-state block of $\beta4_{154–167}$, a slower time frame was used in B, which was recorded ∼30 min after the pipette break-in. (C) The decaying phase of the current traces at 1 mM $\beta4_{154–167}$ was fitted by a single exponential function with a time constant, τ. The τ value was inverted and plotted against the corresponding voltage ($n = 6$ except at −10 mV, where $n = 3$). Error bars represent SEM.

concentration (Fig. 2 A; $n = 5$). The data were fitted by a linear regression and yielded on and off rate values of 10.1 $\mu M^{-1}s^{-1}$ and 49.1 $s^{-1}$, respectively. The calculated equilibrium dissociation constant ($K_D = k_{off}/k_{on}$) was 4.9 μM. For comparison, the estimated values for the ShB peptide in Shaker $K^+$ channels at 50 mV are 4.7 $\mu M^{-1}s^{-1}$, 13.8 $s^{-1}$, and 2.9 μM for $k_{on}$, $k_{off}$, and $K_D$, respectively (Murrell-Lagnado and Aldrich, 1993), or approximately two, four, and two times smaller than those of $\beta4_{154–167}$ in hNav1.5-CW $Na^+$ channels.

At 0.5 mM $\beta4_{154–167}$, the decay of the current has a time constant of ∼0.3 ms, which overlapped the activation time course. The half-time to reach the peak amplitude shown in Fig. 1 A is ∼0.33 ms. Fig. 2 B shows that at the concentration ranging from 0.5 to 2 mM, 1/τ values were nearly constant at ∼3,000 $s^{-1}$. This phenotype implies that when the peptide concentration is ≥0.5 mM, channel activation limits the on rate of the $\beta4_{154–167}$ block. Mathematical simulation of this phenomenon will be given in the Discussion.

### Voltage Dependence of the Time-Dependent Block by $\beta4_{154–167}$

The family of hNav1.5-CW $Na^+$ currents at various voltages in the absence (Fig. 3 A) and presence of $\beta4_{154–167}$ peptide (Fig. 3 B) showed an apparent voltage dependence of the time-dependent block by 125 μM $\beta4_{154–167}$, particularly at voltages ≥20 mV. This voltage-dependent phenotype was found at all $\beta4_{154–167}$ concentrations (25 μM–2 mM). The time-dependent block of these currents could be fitted by a single exponential function from −50 to 80 mV. The time constant was inverted (1/τ) and plotted against voltage. Fig. 3 C shows that the value of 1/τ is strongly voltage dependent from 20 to 80 mV in the presence of 1 mM $\beta4_{154–167}$. At this voltage range, the relationship is linear (Fig. 3 C, dotted line): the larger the voltages, the faster the time constants. At voltage <10 mV, the time-dependent block deviates from the dotted line (Fig. 3 C) and becomes less voltage dependent. Control currents without peptide indicated that minimal inactivation occurred at voltages greater than −10 mV. However, a greater residual fast inactivation appeared in −50 to −20 mV (Fig. 3 A; Wang and Wang, 2005). The reason for this phenotype in control traces at voltages less than −20 mV is not clear. Thus, the time-dependent block may be even less than what we observed at less than −20 mV in Fig. 3 (B and C) because of the presence of residual fast inactivation. We conclude that under our experimental conditions, the time-dependent block of the open $Na^+$ channel becomes progressively stronger when the voltage is >20 mV but is weak at <10 mV.

### Altered Tail Currents at −140 mV in the Presence of $\beta4_{154–167}$

In current traces shown in Figs. 1 and 3, tail currents seemed to decay slower in the presence of 125 μM $\beta4_{154–167}$ (Fig. 1, A vs. B; and Fig. 3, A vs. B). A fast time frame, however, is needed to clearly resolve tail current kinetics. After the pipette break-in, outward inactivation-deficient $Na^+$ currents at a test pulse of 50 mV again increased during the initial dialysis (Fig. 4 A). At the end of the test pulse, these outward currents became inward when the membrane voltage was switched to −140 mV. During the rapid deactivation of the open $Na^+$ channel (Fig. 4 A), these inward tail currents decayed rapidly, which was well fitted by a single exponential function with a τ value of 144 μs. This τ value was similar to that without peptide present ($\tau = 132 \pm 4$ μs; $n = 5$). Although the time-dependent block by β4 peptide at 1 mM continued to develop during the test pulse, both the decay of the tail current and its peak amplitude were also progressively slowed and reduced, resulting in a crossover phenotype (Fig. 4 B; τ = 448 μs for 15-min trace).

If the slowed tail current is caused by the unbinding of β4 peptide upon repolarization (Scheme 2), varying the duration of the test pulse (which enhances the binding of β4 peptide) should affect the tail current kinetics.

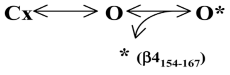


(SCHEME 2)

Therefore, we used such a pulse protocol and measured their corresponding tail current in the presence

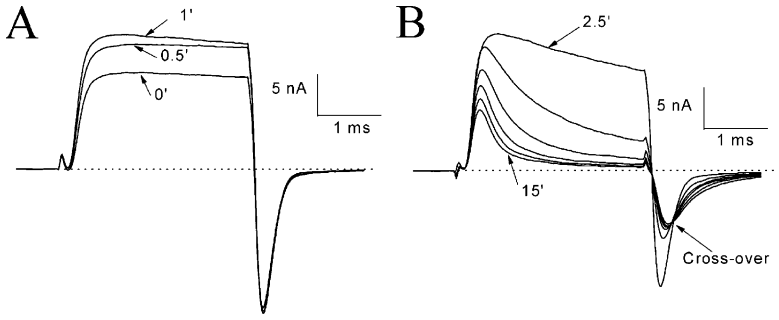


**Figure 4.** Altered tail currents by 1 mM $\beta4_{154–167}$ after pipette break-in. (A) Initial run-up of inactivation-deficient $Na^+$ currents at 50 mV under the whole-cell configuration. This phenomenon was the same as shown in Fig. 1 A except with a faster time frame. The tail currents decayed rapidly with a $\tau$ value of 144 μs. (B) As the time-dependent block continued to develop during the test pulse, the tail current also decayed more slowly. The arrow shows the tail current traces crossing over.

of 1 mM $\beta4_{154–167}$ (Fig. 5 A). The decay of the tail currents and the area under the current trace (3 ms) were measured. Superimposed tail currents (Fig. 5 B) show clear differences in tail current kinetics. The $\tau$ for trace 1 was 328 μs (area under the trace = 4.784 nA × ms), whereas the $\tau$ value for trace 15 was 667 μs (area under trace = 6.393 nA × ms). The $\tau_{P15}/\tau_{P1}$ ratio of tail currents was 1.98 ± 0.02 ($n$ = 5). This result indicates that as more $Na^+$ currents are blocked (O→O* in forward reaction; Scheme 2) during the test pulse, their tail currents become slower in kinetics (O*→O→C in backward reaction). Thus, the O* complex produced two apparent phenotypes on the tail current kinetics: it delayed the time to reach its peak, and it slowed the decay of the tail current. The first phenotype suggests that the activation gate cannot close the pore rapidly when the peptide is bound. The second phenotype suggests that a small fraction of O* continues to dissociate even after the tail reaches its peak. The effects on inactivation-deficient mutant $Na^+$ currents by $\beta4_{154–167}$ peptide did not appear to be isoform specific. Similar tail current phenotypes were observed in the rat skeletal muscle inactivation-deficient rNav1.4-WCW mutant channels (unpublished data).

### Resurgent $Na^+$ Currents Near the Activation Threshold

The altered kinetics in tail currents suggests that the activation gate may not be able to close the channel rapidly (deactivation) when the peptide is bound. If this is true, what conditions will favor the appearance of resurgent tail $Na^+$ currents upon repolarization? Scheme 2 shows that depolarization favors the forward reaction to reach O and eventually to form the O* complex, which results in the time-dependent block. Repolarization to −140 mV then favors the dissociation of the O* complex as well as the normal deactivation (fast tail currents; O→C). At the activation threshold, however, O↔C transition will be generally slow and reversible. If dissociation of the O* complex remains fast, we should observe robust resurgent currents at voltages near the activation threshold. Therefore, with this reasoning, we measured the resurgent $Na^+$ currents at various membrane voltages. After the time-dependent block by 125 μM $\beta4_{154–167}$ developed fully during the test pulse, a large resurgent current emerged when the voltage was switched to −80 mV (Fig. 6 A). The current increased rapidly to reach its peak and then decayed slowly ($\tau$ = 10.8 ± 2.2 ms; $n$ = 6). This slow decay of the resurgent $Na^+$ current could be partly attributed to the slow and reversible closing (deactivation) of the open $Na^+$ channels (O↔C transition)

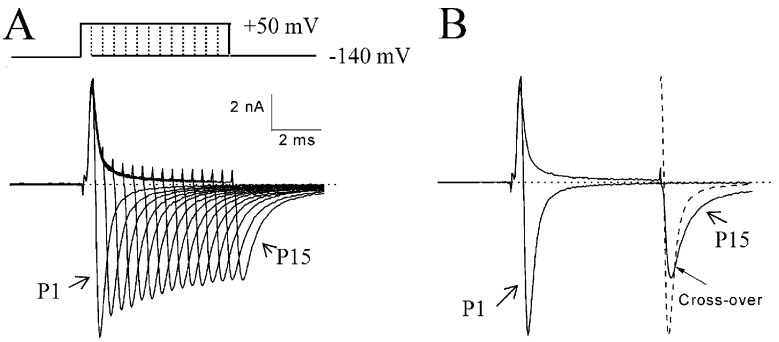


**Figure 5.** Tail current kinetics versus the duration of the test pulse. (A) Superimposed $Na^+$ currents were recorded using a test pulse protocol with duration varying from 0.4 (trace P1) to 6 ms (trace P15) with a 0.4-ms step (top). The pipette solution contained 1 mM $\beta4_{154–167}$. The $\tau$ values of tail currents were measured at 327 ± 18 μs and 649 ± 33 μs for traces P1 and P15, respectively ($n$ = 5). (B) Traces P1 and P15 recorded from the first pulse and from the 15th pulse were compared side by side. Although most of the outward currents in trace P15 were blocked by $\beta4_{154–167}$, large tail currents emerged after the test pulse. The dashed line shows that the tail current from trace P1 reached its peak earlier and decayed faster than that from trace P15. The arrow shows the two traces crossing over. The area under the tail current for trace 15 was larger than that for trace 1. Holding potential was set at −140 mV.

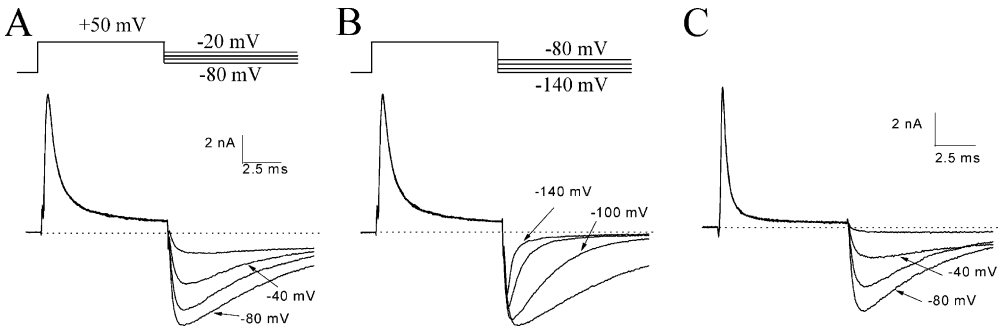


**Figure 6.** Resurgent $Na^+$ currents near the activation threshold. (A) Tail currents were recorded at voltages ranging from −80 to −20 mV with a 20-mV step (top) in inactivation-deficienthNav1.5-CW mutant channels and were superimposed. The pipette contained 125 μM $\beta4_{154–167}$. Resurgent $Na^+$ currents were robust and long lasting with a τ value of 11.5 ms (10.8 ± 2.2 ms; $n = 6$) at −80 mV. (B) Tail currents were recorded in the same cell as shown in A at voltages ranging from −140 to −80 mV with a 20-mV step (top) and were superimposed. The decay of the tail currents was highly dependent on this voltage range. (C) Robust and long-lasting resurgent currents were detected near the activation threshold with the pipette containing 2 mM acetyl-KIFMK-amide. The pulse protocol was the same as shown in A (top). This experiment was repeated in five cells with similar results.

at −80 mV. The rapid rising phase (τ = 232 ± 20 μs; $n = 6$), on the other hand, is mostly caused by the rapid dissociation of the peptide from its binding site. Fig. 6 B shows the resurgent currents from −140 to −80 mV. The rising phase of resurgent tail $Na^+$ currents was not strongly voltage dependent. Therefore, the rising phases of resurgent tail $Na^+$ currents are likely governed by the rapid unbinding of $\beta4_{154–167}$ peptide. The peptide does not bind strongly with the inactivation-deficient $Na^+$ channel effectively at voltages less than −20 mV, as indicated by its weak time-dependent block (Fig. 3 B) and by the peptide-induced large resurgent tail current (Fig. 6, A and B).

We also tested whether the inactivation peptide acetyl-KIFMK-amide can induce resurgent $Na^+$ currents. As of yet, there is no report indicating that acetyl-KIFMK-amide generates resurgent tail currents (Eaholtz et al., 1994, 1999; Tang et al., 1996; Grieco et al., 2005). Fig. 6 C shows that acetyl-KIFMK-amide at 2 mM induces large resurgent tail $Na^+$ currents comparable with those described in Fig. 6 A with $\beta4_{154–167}$. This phenomenon is interesting because it implies that the $Na^+$ channel with the weakened fast inactivation particle, such as in many genetic diseases (Cannon, 1996), could, in theory, also induce resurgent $Na^+$ currents under appropriate conditions.

### Lack of the Use-Dependent Block by $\beta4_{154–167}$ Peptide

To investigate the use-dependent block of $\beta4_{154–167}$, we applied repetitive pulses at 50 mV for 20 ms at 1 Hz and recorded $Na^+$ currents (Fig. 7 A). Both the peak outward currents and peak inward tail currents were measured, normalized, and plotted against the pulse number (Fig. 7 C; open and closed circles, respectively). We found little additional use-dependent block of both the peak and tail currents. The decay of the tail currents was well fitted by an exponential decay with τ = 1.08 ± 0.11 ms ($n = 6$; measured at pulse 1). Under identical conditions, the inactivation peptide acetyl-KIFMK-amide produced additional use-dependent block on the outward peak as well as the inward tail currents by ∼65% (Fig. 7, B and C; open and closed triangles). This use-dependent phenotype for acetyl-KIFMK-amide in hNav1.5-CW inactivation-deficient mutant $Na^+$ channels has been reported previously (Wang and Wang, 2005) and is clearly different from that of $\beta4_{154–167}$. To account for such a use-dependent phenomenon, Eaholtz et al. (1999) suggested that there is a second binding site for acetyl-KIFMK-amide in the pore. By this comparison, there appears to be no second binding site for $\beta4_{154–167}$ peptide within the pore. Interestingly, the tail currents induced by acetyl-KIFMK-amide decayed with a τ value of 0.27 ± 0.02 ms ($n = 5$), or four times faster than that of $\beta4_{154–167}$.

We subsequently tested this peptide dissociation phenotype using the two-pulse protocol shown in Fig. 8 A with a 10-ms interval. The peak current amplitude at the second pulse was nearly the same as that at the first pulse (Fig. 8 A; dashed line). Evidently, the unblocking of $\beta4_{154–167}$ occurred rapidly at −140 mV and probably reached its completion within 10 ms. Under identical conditions, the unblocking of acetyl-KIFMK-amide also occurred rapidly as shown in Fig. 8 B. Thus, for a short pulse of 3 ms, acetyl-KIFMK-amide elicited significantly less use-dependent block during repetitive pulses (28.5 ± 0.4%; $n = 5$ with the fitted τ = 14.5 pulses) than with a long pulse of 20 ms (Fig. 7 B; 62.4 ± 3.1%; $P < 0.001$). In fact, repetitive pulses at 50 mV for 1 ms at 1 Hz produced minimal use-dependent block (15.5 ± 0.4%; $n = 5$ with the fitted τ = 27.1 pulses). Evidently, the longer the pulse duration, the stronger the use-dependent block; this phenomenon suggests that the bound acetyl-KIFMK-amide could be moved to its second binding site during prolonged depolarization. In contrast, $\beta4_{154–167}$ does not move further to such a second binding site under identical conditions. It is noteworthy that even with a short test pulse, the tail current induced by 2 mM $\beta4_{154–167}$ decayed slower than that induced by 2 mM

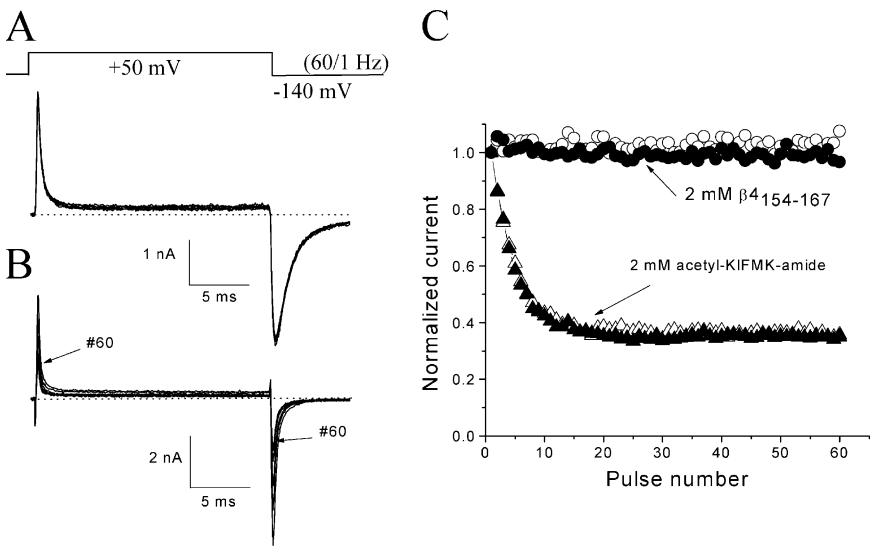


**Figure 7.** Use-dependent block by $\beta4_{154–167}$ versus by acetyl-KIFMK-amide. (A) Superimposed currents were recorded during repetitive pulse (top; 50 mV/20 ms at 1 Hz). Current traces corresponded to the pulse numbers 1, 3, 5, 10, 20, 30, 40, 50, and 60. The pipette solution contained 2 mM $\beta4_{154–167}$. (B) Superimposed currents were recorded under an identical protocol except the pipette solution contained 2 mM acetyl-KIFMK-amide. (C) Peak outward $Na^+$ currents (open symbols) and peak inward tail currents (closed symbols) as shown in A and B were measured, normalized with respect to the peak value obtained from pulse 1, and plotted against the corresponding pulse number. Open and closed circles represent data from A in the presence of 2 mM $\beta4_{154–167}$, whereas open and closed triangles are data from B with 2 mM acetyl-KIFMK-amide. Experiments were repeated in five separate cells with similar results. Use-dependent block of peak currents was minimal in the presence of 2 mM $\beta4_{154–167}$ (2.9 ± 1.6%; $n = 6$), whereas the use-dependent block in 2 mM acetyl-KIFMK-amide was 62.4 ± 3.1% ($n = 5$).

acetyl-KIFMK-amide (0.67 ± 0.04 ms vs. 0.23 ± 0.02 ms; $n = 6$). This phenotype implies that acetyl-KIFMK-amide dissociates faster than $\beta4_{154–167}$ from the $Na^+$ channel upon repolarization.

### Competition between the β4 Peptide and the Inherent Fast Inactivation Particle

The intrinsic fast inactivation particle blocks the open $Na^+$ channel rapidly (Aldrich et al., 1983). An elongated form of a large ShB peptide (i.e., the first 20 amino acids on the $NH_2$ terminus of the Shaker channel) could enter deep into the inner cavity of the $K^+$ channel as suggested by Zhou et al. (2001). According to the foot-in-the-door model for fast inactivation (Armstrong, 1981), the inactivated channel does not carry tail currents during deactivation because the activation gate (door) is partially closed before the withdrawal of the inactivation particle (foot). Fig. 9 A shows the representative traces of the wild-type hNav1.5 $Na^+$ currents. The tail current amplitude is inversely proportional to the degree of fast inactivation during the pulse. The tail current through normal open $Na^+$ channels decayed rather rapidly with a $\tau$ value of 94 ± 12 μs ($n = 8$ at pulse P1).

With 1 mM $\beta4_{154–167}$ peptide in the pipette solution, this proportionality in the peak and tail currents was no longer true (Fig. 9 B). Also evident in this figure is that the decaying phase of the $Na^+$ currents during the test pulse has a faster time constant ($\tau = 151 \pm 15$ μs; $n = 8$) than that without $\beta4_{154–167}$ peptide ($\tau = 580 \pm 13$ μs; $n = 6$; $P < 0.001$; Fig. 9 A), suggesting that during depolarization, $\beta4_{154–167}$ competes with the binding of the intrinsic inactivation particle. In addition, a peptide-induced tail current appeared upon repolarization. Near the activation threshold, resurgent $Na^+$ currents appeared robust and long lasting (Fig. 9 C). Again, these resurgent tail currents could be attributed mostly to the rapid dissociation of the bound $\beta4_{154–167}$ peptide. Such a tail current is absent from wild-type $Na^+$ channels without the β4 subunit. These phenotypes are consistent with the hypothesis that the inactivation particle and the $\beta4_{154–167}$ peptide are mutually exclusive in binding to their receptors (Raman and Bean, 2001).

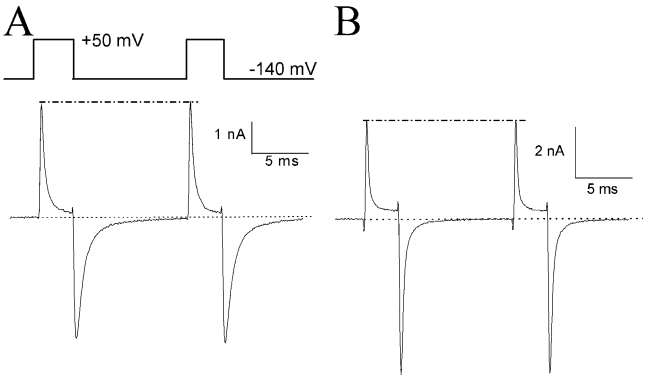


**Figure 8.** Rapid unblocking of $\beta4_{154–167}$ and acetyl-KIFMK-amide upon repolarization. (A) Unblocking of $\beta4_{154–167}$ occurred within 10 ms as shown by a two-pulse protocol (top). The pipette solution contained 2 mM $\beta4_{154–167}$. The interval was set for 10 ms between two pulses. The tail currents decayed rapidly to the baseline during this interval. Peak currents generated by these two pulses remained the same (dashed line). (B) Similar results were found in the presence of 2 mM acetyl-KIFMK-amide under identical conditions. Experiments in A and B were each repeated in six cells with the same results.

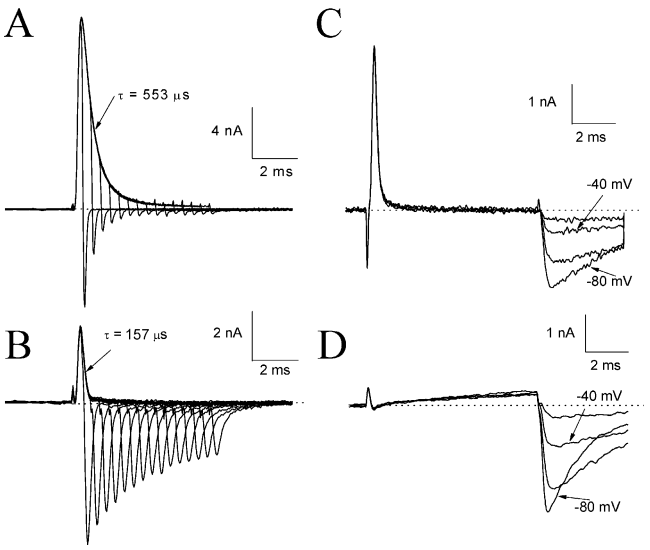


**Figure 9.** Competition between $\beta4_{154–167}$ and the intrinsic fast inactivation particle. Current traces of wild-type $Na^+$ channels in the absence (A) and presence (B) of 1 mM $\beta4_{154–167}$ were recorded at 50 mV with duration varying from 0.4 to 6.0 ms and were superimposed. The pulse protocol was the same as shown in Fig. 5 A. The outward current in A and B decayed with a $\tau$ value of 0.157 and 0.553 ms, respectively. Evidently, the time-dependent block induced by $\beta4_{154–167}$ also occurred in wild-type $Na^+$ channels. The tail current of trace 15 in A (P15) was barely detectable, but in B was quite large and significantly slower in its decay kinetics when 1 mM $\beta4_{154–167}$ was present. Resurgent currents were recorded from wild-type $Na^+$ channels at voltages ranging from −80 to −20 mV with a 20-mV step (C). The pulse protocol is the same as shown in Fig. 6 A. The pipette solution contained 1 mM $\beta4_{154–167}$. Experiments were repeated in eight cells with similar results under the reversed $Na^+$ gradient condition (65 mM $Na^+$ ions in the bath and 130 mM $Na^+$ ions in the pipette). (D) Current traces were recorded in the presence of 1 mM $\beta4_{154–167}$ as described in C except that the bath and pipette solutions had 130 and 13 mM $Na^+$ ions, respectively. Although $Na^+$ currents at 50 mV were minimal under the normal $Na^+$ gradient condition, the resurgent currents remained robust near the activation threshold. This experiment was repeated in five cells with similar results.

Under a normal $Na^+$ gradient (e.g., 130 mM of external $Na^+$ ions and 13 mM of internal $Na^+$ ions), competition between the intrinsic fast inactivation particle and $\beta4_{154–167}$ peptide could not be observed readily during the 50-mV pulse (Fig. 9 D). The $Na^+$ currents were small and difficult to identify under this condition because the pulse voltage was near the reversal potential (~60 mV) and because a nonlinear leak was often present. However, resurgent tail $Na^+$ currents were clearly evident near the activation threshold under the normal $Na^+$ gradient and resembled those under the reversed gradient shown in Fig. 9 C, confirming again that competition occurs between $\beta4_{154–167}$ peptide and the fast inactivation particle.

### Changes in the Time-Dependent Block by External $Na^+$ Ions

Afshari et al. (2004) reported that in cerebellar neurons, external $Na^+$ ions could knock off the endogenous open-channel blocker, which induces resurgent currents. We tested whether a similar knock-off phenomenon can be detected in hNav1.5 $Na^+$ channels. The time-dependent block of outward $Na^+$ currents at 50 mV was measured under various external solutions containing 0, 65, and 130 mM $Na^+$ ions. We found that the $\tau$ value for $\beta4_{154–167}$ at 2 mM changed only slightly under these conditions (Fig. 10 A). The ratio of $\tau_{65}/\tau_0$ and $\tau_{130}/\tau_0$ was 1.09 ± 0.03 ($n = 7$) and 1.30 ± 0.04 ($n = 7$), respectively. These averaged values do deviate from unity significantly ($P < 0.05$). The peak currents were superimposed before and after the solution exchange. Tail currents were small or nonexistent in 0 mM $Na^+$ ions, whereas tail currents were larger in external 130 mM than those in 65 mM $Na^+$ ions. There were no significant changes in the tail current kinetics. Because the $\tau$ value for the time-dependent block by $\beta4_{154–167}$ saturated at 2 mM and was severely limited by channel activation (Fig. 2 B), we also measured the $Na^+$ effect at lower concentrations of $\beta4_{154–167}$.

Unlike at 2 mM, the $\tau$ values for $\beta4_{154–167}$ at 125 μM were notably altered by external $Na^+$ ions. Fig. 10 B shows that a decrease in external $Na^+$ ions accelerates the time-dependent block, whereas an increase in external $Na^+$ ions decelerates it. The ratio of $\tau_{65}/\tau_0$ and $\tau_{130}/\tau_0$ was 1.28 ± 0.05 ($n = 5$) and 1.81 ± 0.06 ($n = 5$), respectively. These ratios deviate from unity significantly ($P < 0.05$). In addition, the magnitude of steady-state block was higher at 0 mM $Na^+$ ions and lower at 130 mM $Na^+$ ions. These phenotypes were consistently found in cells with internal $\beta4_{154–167}$ concentrations ranging from 25 to 250 μM. Evidently, external $Na^+$ ions reduce internal $\beta4_{154–167}$ binding strongly during depolarization. Interesting, unblocking of $\beta4_{154–167}$ upon repolarization was not affected, as shown by similar kinetics of the tail currents (Fig. 10 B). This result implies that an increase in the $Na^+$ concentration slows primarily the on rate binding of $\beta4_{154–167}$. However, cautions must be taken in interpreting these results because the effect of external $Na^+$ ions may be partially concealed at high $\beta4_{154–167}$ concentrations, probably as a result of the saturated $\tau$ values shown in Fig. 2 B.

### Minimal Time-Dependent Block of BTX-Modified $Na^+$ Currents by $\beta4_{154–167}$

BTX is a potent $Na^+$ channel activator that eliminates the fast inactivation of voltage-gated $Na^+$ channels (Catterall, 1980; Wang and Wang, 2003; for review see Strichartz, et al., 1987). To determine whether BTX also eliminates the time-dependent block induced by peptide blockers, we included 4 μM BTX in the pipette solution along with 2 mM acetyl-KIFMK-amide or 1 mM β4 peptide. With infrequent stimuli applied every 30 s, peptide-induced phenotypes, such as the time-dependent block during the test pulse and the large tail currents upon repolarization, were similar to those found without BTX. With repetitive pulses of 50 mV for 20 ms at 2 Hz, however, BTX began to bind to the open

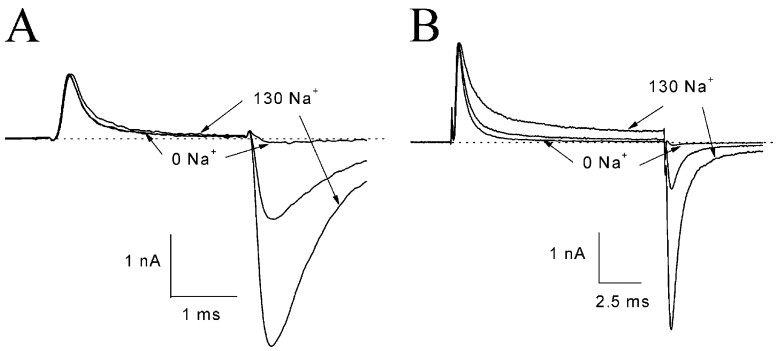


**Figure 10.** Changes in the $\beta4_{154–167}$ time-dependent block by external $Na^+$ concentration. (A) Superimposed current traces of hNav1.5-CW mutant $Na^+$ channels were recorded with a bath solution containing 130, 65, or 0 mM $Na^+$ ions and normalized with respect to the outward peak value. The $\tau$ values for 0, 65, and 130 mM $Na^+$ ions were 0.277 ($\tau_0$), 0.276 ($\tau_{65}$), and 0.334 ms ($\tau_{130}$), respectively. The pipette solution contained 2 mM $\beta4_{154–167}$. A minimal tail current was present with 0 mM external $Na^+$ ions, whereas a large tail was found with 65 and 130 mM external $Na^+$ ions. (B) Currents were recorded under an identical protocol, except the pipette solution contained 125 μM $\beta4_{154–167}$. The $\tau$ values for 0, 65, and 130 mM $Na^+$ ions were 0.540, 0.697, and 0.952 ms, respectively. These experiments were repeated in five to seven cells.

$Na^+$ channel, and maintained BTX-modified $Na^+$ currents became evident. Fig. 11 (A and B) shows the current family at various voltages in wild-type BTX-modified $Na^+$ channels after 2,000 repetitive pulses. Fast inactivation was severely impaired, and large $Na^+$ currents were activated even at −80 mV. However, unlike traces shown in Figs. 7 and 8, little time-dependent block was found in these current traces despite the presence of 2 mM acetyl-KIFMK-amide and 1 mM $\beta4_{154–167}$. The ratios of the maintained versus peak current at 50 mV were measured at 90.2 ± 3.9% ($n$ = 6) and 89.2 ± 4.3% ($n$ = 5) for experiments shown in Fig. 11 (A and B, respectively). Similar results were found in BTX-modified inactivation-deficient mutant $Na^+$ channels during a prolonged depolarization (Fig. 11 C); these currents again showed minimal time-dependent block by 1 mM $\beta4_{154–167}$. In contrast, the time-dependent block by $\beta4_{154–167}$ peptide was present before repetitive pulses. Evidently, the BTX-modified open $Na^+$ channel becomes resistant to $\beta4_{154–167}$ peptide and to acetyl-KIFMK-amide block. This result suggests that BTX prevents the intrinsic fast inactivation particle acetyl-KIFMK-amide and $\beta4_{154–167}$ from binding with their receptors.

### Are hNav1.5-CW/F1760K Mutant $Na^+$ Channels Resistant to $\beta4_{154–167}$ Block?

The peptide-resistant phenotype in BTX-modified $Na^+$ channels implies that the BTX receptor may overlap the $\beta4_{154–167}$ receptor. This, in turn, raises a possibility that mutations at the BTX-binding site may also affect $\beta4_{154–167}$ peptide binding. Therefore, we expressed BTX-resistant hNav1.5-CW/F1760K channels in HEK293t cells and examined their sensitivity toward $\beta4_{154–167}$ peptide. The conserved F residue in hNav1.5-F1760 has been known to form a part of the local anesthetic receptor as well as the BTX receptor within the inner cavity of the $Na^+$ channel (Ragsdale et al., 1994; Linford et al., 1998; Wang and Wang, 2003). Acetyl-KIFMK-amide may also interact with this aromatic residue (Wang and Wang, 2005). The location of this F residue is at the middle of D4S6, adjacent to the putative gating hinge (a serine residue; i.e., hNav1.5-S1759).

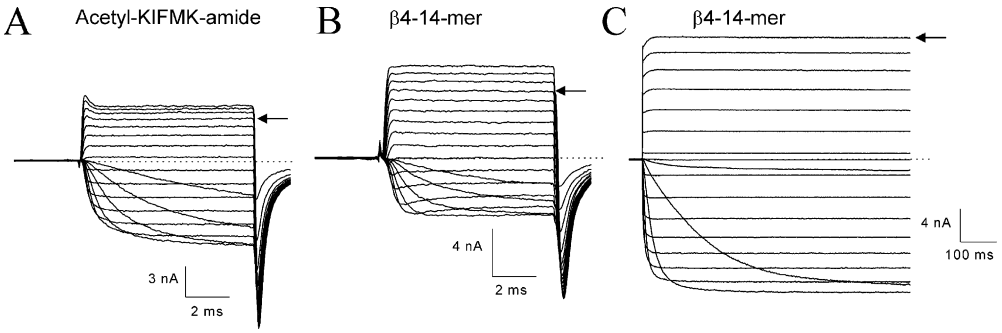


**Figure 11.** Absence of time-dependent block by $\beta4_{154–167}$ in BTX-modified wild-type or hNav1.5-CW mutant $Na^+$ channels. Repetitive pulses (50 mV/20 ms at 2 Hz) were applied 2,000 times after the pipette break-in. The families of BTX-modified wild-type $Na^+$ channels (A and B) or hNav1.5-CW mutant channels (C) were then recorded and superimposed. Current traces corresponding to 50 mV were labeled by arrows. Besides 4 μM BTX, the pipette solution also contained either 2 mM acetyl-KIFMK-amide (A) or 1 mM $\beta4_{154–167}$ (B and C). The time frame was recorded ∼50× slower in C than that in A and B. The bath solution contained 130 mM $Na^+$ ions (A) or 65 mM $Na^+$ ions (B and C). Holding potential was set at −140 mV. Experiments were repeated in five to six cells with similar results.

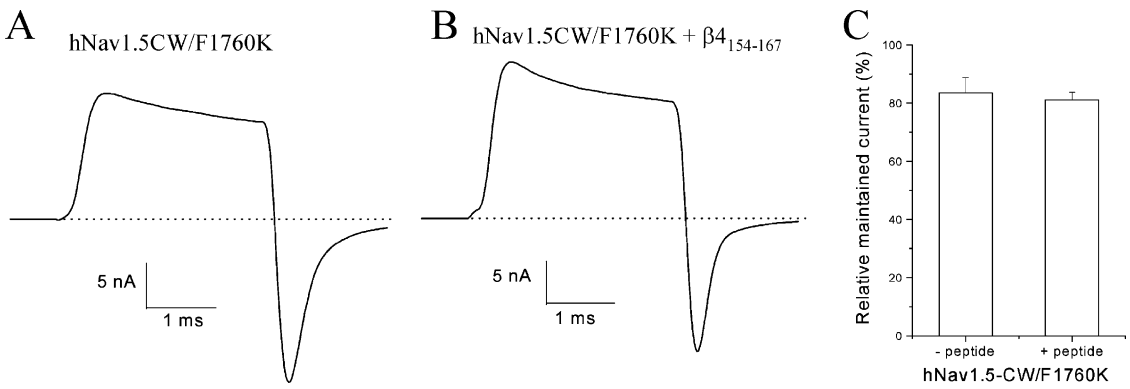


**Figure 12.** A $\beta4_{154–167}$-resistant phenotype in hNav1.5-CW/F1760K mutant $Na^+$ channels. Traces of hNav1.5-CW/F1760K mutant $Na^+$ currents at 50 mV were recorded after >30 min under whole-cell configuration in the absence (A) or presence (B) of 1 mM $\beta4_{154–167}$ within the pipette solution. The $\tau$ values for the tail current decay were measured at 190.6 ± 30.0 μs and 219.7 ± 19.6 μs ($n = 5$) without and with 1 mM $\beta4_{154–167}$, respectively. The difference in $\tau$ values is not statistically significant (P = 0.44). The maintained currents at the end of the test pulse in A and B were measured, normalized with the peak current amplitude, and plotted in C ($n = 5$). No statistical difference was found in these measurements. Error bars represent SD.

Fig. 12 (A and B) shows traces of hNav1.5-CW/F1760K currents in the absence and presence of 1 mM $\beta4_{154–167}$ peptide, respectively. The inactivation-deficient phenotype of hNav1.5-CW/F1760K channels is comparable with that of hNav1.5-CW counterparts. Unlike in hNav1.5CW channels, however, we did not observe a rapid time-dependent block by $\beta4_{154–167}$ peptide in hNav1.5-CW/F1760K channels after internal dialysis for >30 min (Fig. 12 B). The relative maintained currents at the end of the test pulse in these mutant channels with the peptide remain the same as those without the peptide (Fig. 12 C; P = 0.68). In addition, we observed no significant changes in tail current kinetics during dialysis. Preliminary scanning of rNav1.4-WCW/F1579K $Na^+$ currents at 50 mV also showed that these F1579K mutant $Na^+$ channels were resistant to $\beta4_{154–167}$ peptide at 1 mM. Our data thus reveal a locus critical for $\beta4_{154–167}$ binding. Substitution of phenylalanine (F) with lysine (K) at this conserved D4S6 site appears to render both hNav1.5 and rNav1.4 isoforms not only resistant to LAs and BTX but also to $\beta4_{154–167}$ peptide.

## DISCUSSION

We have described several $\beta4_{154–167}$-induced phenotypes in wild-type and inactivation-deficient mutant hNav1.5 $Na^+$ channels. Many of these $\beta4_{154–167}$-induced phenotypes resemble those found in native neuronal $Na^+$ channels from Purkinje neurons (Grieco et al. 2005). First, cardiac $Na^+$ channels can carry resurgent $Na^+$ currents in the presence of intracellular $\beta4_{154–167}$. Second, $\beta4_{154–167}$ elicits a conspicuous time-dependent block at 50 mV. Third, $\beta4_{154–167}$ dissociates rapidly from its receptor upon repolarization. Fourth, a fast inactivation peptide, acetyl-KIFMK-amide, induces resurgent $Na^+$ currents almost as robustly as $\beta4_{154–167}$. Fifth, BTX eliminates the time-dependent block elicited by $\beta4_{154–167}$. Finally, lysine substitution of a conserved phenylalanine residue at D4S6 renders the channel resistant to $\beta4_{154–167}$. We conclude that the hNav1.5 $Na^+$ channel expressed in HEK293t cells is applicable to study the pharmacological actions of $\beta4_{154–167}$. This in vitro expression system also provides the means for $\beta4_{154–167}$ receptor mapping by site-directed mutagenesis. The origin of resurgent $Na^+$ currents and the underlying mechanism of $\beta4_{154–167}$ actions in Purkinje neurons have been documented in detail by Raman and Bean (2001) and Grieco et al. (2005). In the context of these landmark studies, the significance of $\beta4_{154–167}$-induced phenotypes found in cardiac hNav1.5 channels is discussed in the following paragraphs.

### Cardiac Nav1.5 $Na^+$ Channels can Carry Resurgent $Na^+$ Currents

Resurgent $Na^+$ currents in dissociated cerebellar Purkinje neurons are probably carried by neuronal Nav1.6 $Na^+$ channels (Raman, et al., 1997). Our results showed that cardiac and skeletal muscle inactivation-deficient mutant $Na^+$ channels also carry robust resurgent $Na^+$ currents in the presence of $\beta4_{154–167}$. Evidently, resurgent currents can be generated in an in vitro expression system without dissociated neurons. It is likely that resurgent $Na^+$ currents are not isoform specific, and most $Na^+$ channel isoforms can carry resurgent $Na^+$ currents. Transcripts of β4 have been found in the central nervous system, dorsal root ganglion, heart, and skeletal muscle (Yu et al., 2003). Immunostaining shows that β4 and Nav1.5 are colocalized at intercalated disks in ventricular myocytes (Maier et al., 2004). Whether the β4 subunit at intercalated disks can induce resurgent $Na^+$ currents in vivo remains to be examined. Such a question has not yet been resolved in dissociated Purkinje

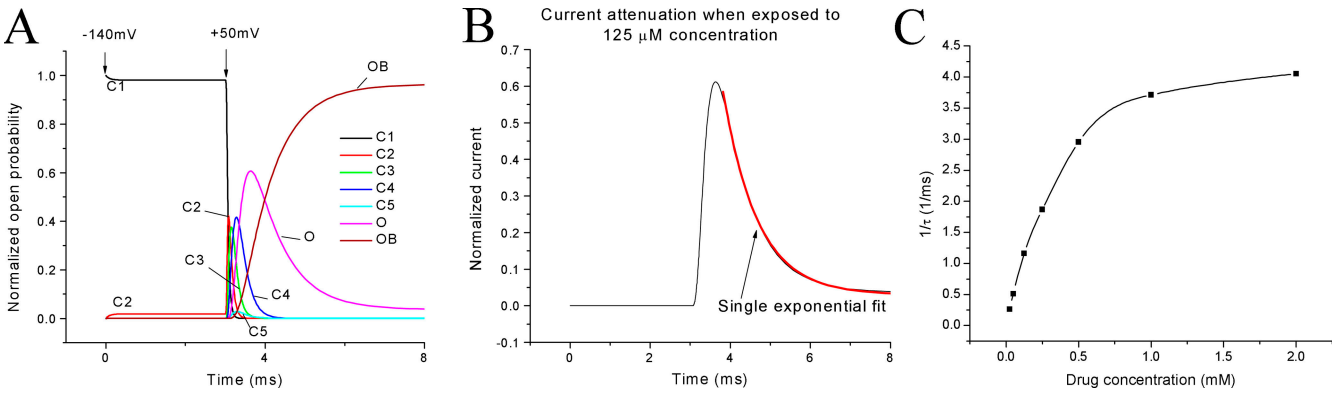


**Figure 13.** Computer simulation of the time-dependent block by $\beta4_{154–167}$ at 50 mV. (A) Normalized open probability against time is shown. Normalized probabilities for transient closed and open blocked states are also included. Data were generated by the MATLAB software according to Scheme 1 with $\alpha = 1.6\ e^{V/40}$, $\beta = 0.3\ e^{-V/40}$, $\gamma = 50\ e^{V/100}$, and $\delta = 0.6\ e^{-V/25}$, where V is in millivolts. The $\beta4_{154–167}$ concentration is set at 125 μM; rate constants are the same as described in Fig. 2 A. (B) The time-dependent block during the pulse can be fitted by a single exponential function, $\tau = 0.86$ ms. (C) The plot of $1/\tau$ against $\beta4_{154–167}$ concentration shows a nonlinear relationship. The difference on the saturation level between Fig. 2 B and Fig.13 C is likely inherent because rate constants for binding were extracted by linear regression and because the voltage coefficients were obtained by repetitive approximation.

neurons (Grieco et al. 2005). Coexpression of hNav1.5 and the β4 subunit in HEK293t cells may also help address this question in the future, although a positive result from this approach is by no means guaranteed because the native system could still turn out to require scaffolding proteins or some other accessory proteins to function properly (Bean, 2005).

### $\beta4_{154–167}$ Gains Access to its Receptor Only When the hNav1.5 Channel is Open

Several pieces of evidence support the hypothesis that the receptor for $\beta4_{154–167}$ is inside the pore region of the hNav1.5 channel and that the activation gate governs the receptor accessibility. First, the time-dependent block of inactivation-deficient hNav1.5 $Na^+$ currents at 50 mV (Fig. 1) suggests that $\beta4_{154–167}$ interacts with the open $Na^+$ channel directly as an open-channel blocker (Grieco et al. 2005). Second, external $Na^+$ ions influence the kinetics of the time-dependent block by internal $\beta4_{154–167}$ (Fig. 10 B). Such a phenomenon is often found for open-channel blockers and implies that a knock-off mechanism by external $Na^+$ ions occurs in peptide binding within the pore region (Tang et al. 1996; Afshari et al. 2004). Third, when $\beta4_{154–167}$ concentrations are ≥0.5 mM, the τ value of the time-dependent block becomes saturated (Fig. 2 B). Computer simulation shows that the block by $\beta4_{154–167}$ at 125 μM is well fitted by a single exponential function (Fig.13 B). A nonlinear relationship with a saturation of the $1/\tau$ value at high $\beta4_{154–167}$ concentrations (≥0.5 mM) is observed by simulation (Fig. 13 C). What is the cause for this saturation at high peptide concentrations? We find that as the peptide concentration is raised, the τ value for the time-dependent block becomes faster and increasingly overlaps with the activation time course (Fig. 13 A). In other words, $Na^+$ channels that open late will effectively delay the peptide binding and give the appearance of saturation of the $1/\tau$ value. The results of this mathematical simulation strongly advocate that only the open channel is accessible to the $\beta4_{154–167}$ block.

### $\beta4_{154–167}$ Dissociates Rapidly from its Binding Site in the hNav1.5 Channel upon Repolarization

The occurrence of resurgent tail $Na^+$ currents depends on the rapid dissociation of $\beta4_{154–167}$ from its receptor upon repolarization (Raman and Bean, 2001; Grieco et al., 2005). Resurgent tail $Na^+$ currents are robust and long lasting at the activation threshold (approximately −70 mV) as expected (Fig. 6). Depolarization to −70 mV alone without a conditioning pulse does not elicit large resurgent $Na^+$ currents (Fig. 3). Also, no resurgent $Na^+$ currents are found in wild-type hNav1.5 $Na^+$ channels upon repolarization (Fig. 9 A) because the intrinsic fast inactivation particle does not unbind fast enough (Armstrong, 1981).

A fast inactivation peptide, acetyl-KIFMK-amide, can induce robust resurgent $Na^+$ currents in inactivation-deficient hNav1.5 $Na^+$ channels (Fig. 6 C), indicating that rapid dissociation of this small peptide causes resurgent currents to emerge upon repolarization. A small peptide such as acetyl-KIFMK-amide, however, may be trapped within the pore region by sequential reactions during repetitive pulses (Eaholtz et al., 1999), resulting in the additional use-dependent block of $Na^+$ currents (Fig. 7, B and C). In contrast, a peptide such as $\beta4_{154–167}$ could not be trapped within the inner cavity because of its large size. The rapid block and unblock of $\beta4_{154–167}$ in hNav1.5 channels bears a clear resemblance to the block and unblock of polycyclic blockers in squid $Na^+$ channels (Yeh and Narahashi, 1977; Cahalan and Almers,

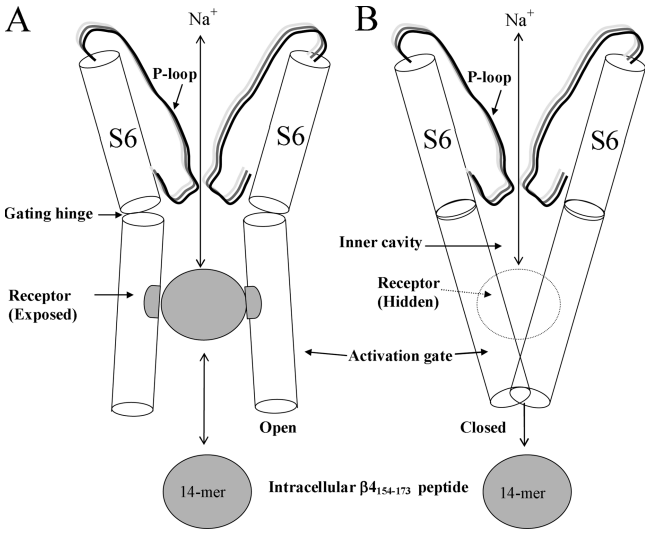


**Figure 14.** A cartoon for the foot-in-the-door model. The pore region of the pseudotetrameric α-subunit $Na^+$ channel is formed by P-loop (S5/S6 linker) and S6 segments from each of four domains (D1–D4). The front and back structures are omitted for clarity. The inner cavity, the putative gating hinge, and the activation gate are labeled. The peptide receptor is exposed for binding (left) when the channel is in the open state (Tikhonov and Zhorov, 2005) and is hidden (right) when the channel is in the closed state (Lipkind and Fozzard, 2000). $\beta4_{154–167}$ is drawn as a ball. The permeation pathway is not large enough to trap $\beta4_{154–167}$ within the inner cavity when the channel is closed. Blocking and unblocking of $\beta4_{154–167}$ within the pore is analogous to the foot-in-the-door model for fast inactivation proposed by Armstrong (1981). However, upon repolarization, the activation gate is partially deactivated before the withdrawal of the intrinsic fast inactivation particle from the channel mouth. In contrast, unbinding of $\beta4_{154–167}$ is rapid upon repolarization, and during this dissociation process the activation gate remains open.

1979). This resemblance can be adequately explained by the foot-in-the-door model (Fig. 14) proposed for the inherent fast inactivation particle (Armstrong, 1981).

### The Whereabouts of the $\beta4_{154–167}$ Receptor in hNav1.5 $Na^+$ Channels

The location of the $\beta4_{154–167}$ receptor may be deduced by the properties of $\beta4_{154–167}$ as an open-channel blocker, by competition studies with other ligands, and by site-directed mutagenesis. $\beta4_{154–167}$ and acetyl-KIFMK-amide peptides act similarly as open-channel blockers in hNav1.5 channels. Both ligands produce strong time-dependent blocking of inactivation-deficient hNav1.5 channels at 50 mV (Fig. 8), and, upon repolarization, they both induce robust resurgent tail $Na^+$ currents near the activation threshold (Fig. 6). The result that $\beta4_{154–167}$ competes with the intrinsic fast inactivation particle for binding with the open pore (Fig. 9, A and B) is consistent with the hypothesis that occupancy of the hNav1.5 channel by $\beta4_{154–167}$ prevents binding of the fast inactivation particle (Raman and Bean, 2001; Grieco et al., 2005), which contains the IFM motif.

Because BTX eliminates fast inactivation, we reason that BTX will also eliminate both acetyl-KIFMK-amide and $\beta4_{154–167}$ binding within the inner cavity by physical exclusion. This prediction is supported by our data (Fig. 11); BTX-modified $Na^+$ channels become resistant to blocking by both peptides. Because the BTX receptor is likely located within the inner cavity (Wang and Wang, 2003), Fig. 14 depicts the putative $\beta4_{154–167}$ binding site, which is drawn between the gating hinge and the S6 COOH-terminal end. The COOH termini of S6s likely form the bundle-crossing site that acts as the activation gate (Fig. 14, right side; Lipkind and Fozzard, 2000; Jiang et al., 2002). The fact that a lysine substitution of a conserved phenylalanine residue (hNav1.5-F1760K) at the middle of the D4S6 segment (1) renders the channel resistant to $\beta4_{154–167}$ (Fig. 12), (2) abolishes the use-dependent block by acetyl-KIFMK-amide, and (3) hinders its time-dependent block (Wang and Wang, 2005) are in agreement with this model.

Could this conserved F1760 residue form a part of receptors for $\beta4_{154–167}$, acetyl-KIFMK-amide, local anesthetics, and BTX? This seems to be a logical explanation for the $\beta4_{154–167}$-resistant phenotype in hNav1.5-F1760K mutant channels. Such an interpretation also agrees with most other $\beta4_{154–167}$-induced phenotypes. Unfortunately, we were unable to rule out several other alternatives. First, a lysine substitution at F1760 could affect $\beta4_{154–167}$ binding allosterically. Second, long-range charge–charge repulsion could occur between lysine (F1760K) and $\beta4_{154–167}$, which has five net positive charges. Third, the $\beta4_{154–167}$ receptor could overlap the BTX receptor only peripherally. These aforementioned scenarios do not require that F1760 interacts with $\beta4_{154–167}$ directly and could place the $\beta4_{154–167}$-binding site near the S6 COOH termini, closer to the intracellular entrance. Interestingly, a similar receptor site near the intracellular mouth has been suggested for the intrinsic fast inactivation particle in a hinged lid model (Catterall, 2000). Further detailed receptor mapping will be needed to delineate the receptor sites for $\beta4_{154–167}$, acetyl-KIFMK-amide, and the fast inactivation particle with the IFM motif. All these open-channel blockers along with BTX appear to be mutually exclusive when bound within the pore region.

We thank Drs. Roland Kallen, William Catterall, and John Daly for providing us with hNav1.5, rβ1, and BTX, respectively.

This work was supported by grants from the National Institutes of Health (GM48090 and HL66076).

Olaf S. Andersen served as editor.

Submitted: 9 September 2005
Accepted: 31 January 2006

## REFERENCES

Afshari, F.S., K. Ptak, Z.M. Khaliq, T.M. Grieco, N.T. Slater, D.R. McCrimmon, and I.M. Raman. 2004. Resurgent Na currents in

four classes of neurons of the cerebellum. *J. Neurophysiol.* 92:2831–2843.

Aldrich, R.W., D.P. Corey, and C.F. Stevens. 1983. A reinterpretation of mammalian sodium channel gating based on single channel recording. *Nature.* 306:436–441.

Armstrong, C.M. 1981. Sodium channels and gating currents. *Physiol. Rev.* 61:644–683.

Armstrong, C.M., and F. Bezanilla. 1977. Inactivation of the sodium channel. II. Gating current experiments. *J. Gen. Physiol.* 70:567–590.

Bean, B.P. 2005. The molecular machinery of resurgent sodium current revealed. *Neuron.* 45:185–187.

Cahalan, M.D., and W. Almers. 1979. Block of sodium conductance and gating current in squid giant axons poisoned with quaternary strychnine. *Biophys. J.* 27:57–73.

Cannon, S.C. 1996. Sodium channel defects in myotonia and periodic paralysis. *Annu. Rev. Neurosci.* 19:141–164.

Catterall, W.A. 1980. Neurotoxins that act on voltage-sensitive sodium channels in excitable membranes. *Annu. Rev. Pharmacol. Toxicol.* 20:15–43.

Catterall, W.A. 2000. From ionic currents to molecular mechanisms: the structure and function of voltage-gated sodium channels. *Neuron.* 26:13–25.

Cota, G., and C.M. Armstrong. 1989. Sodium channel gating in clonal pituitary cells: the inactivation step is not voltage dependent. *J. Gen. Physiol.* 94:213–232.

Cummins, T.R., S.D. Dib-Hajj, R.I. Herzog, and S.G. Waxman. 2005. Nav1.6 channels generate resurgent sodium currents in spinal sensory neurons. *FEBS Lett.* 579:2166–2170.

Do, M.T., and B.P. Bean. 2004. Sodium currents in subthalamic nucleus neurons from Nav1.6-null mice. *J. Neurophysiol.* 92:726–733.

Eaholtz, G., T. Scheuer, and W.A. Catterall. 1994. Restoration of inactivation and block of open sodium channels by an inactivation gate peptide. *Neuron.* 12:1041–1048.

Eaholtz, G., A. Colvin, D. Leonard, C. Taylor, and W.A. Catterall. 1999. Block of brain sodium channels by peptide mimetics of the isoleucine, phenylalanine, and methionine (IFM) motif from the inactivation gate. *J. Gen. Physiol.* 113:279–294.

Grieco, T.M., and I.M. Raman. 2004. Production of resurgent current in NaV1.6-null Purkinje neurons by slowing sodium channel inactivation with beta-pompilidotoxin. *J. Neurosci.* 24:35–42.

Grieco, T.M., J.D. Malhotra, C. Chen, L.L. Isom, and I.M. Raman. 2005. Open-channel block by the cytoplasmic tail of sodium channel beta4 as a mechanism for resurgent sodium current. *Neuron.* 45:233–244.

Hamill, O.P., E. Marty, M.E. Neher, B. Sakmann, and F.J. Sigworth. 1981. Improved patch-clamp techniques for high-resolution current recording from cells and cell-free membrane patches. *Pflugers Arch.* 391:85–100.

Jiang, Y., A. Lee, J. Chen, M. Cadene, B.T. Chait, and R. MacKinnon. 2002. The open pore conformation of potassium channels. *Nature.* 417:523–526.

Linford, N.J., A.R. Cantrell, Y. Qu, T. Scheuer, and W.A. Catterall. 1998. Interaction of batrachotoxin with the local anesthetic receptor site in transmembrane segment IVS6 of the voltage-gated sodium channel. *Proc. Natl. Acad. Sci. USA.* 95:13947–13952.

Lipkind, G.M., and H.A. Fozzard. 2000. KcsA crystal structure as framework for a molecular model of the $Na^+$ channel pore. *Biochemistry.* 39:8161–8170.

Maier, S.K., R.E. Westenbroek, K.A. McCormick, R. Curtis, T. Scheuer, and W.A. Catterall. 2004. Distinct subcellular localization of different sodium channel alpha and beta subunits in single ventricular myocytes from mouse heart. *Circulation.* 109:1421–1427.

Murrell-Lagnado, R.D., and R.W. Aldrich. 1993. Interactions of amino terminal domains of Shaker K channels with a pore blocking site studied with synthetic peptides. *J. Gen. Physiol.* 102:949–975.

Ragsdale, D.S., J.C. McPhee, T. Scheuer, and W.A. Catterall. 1994. Molecular determinants of state-dependent block of $Na^+$ channels by local anesthetics. *Science.* 265:1724–1728.

Raman, I.M., and B.P. Bean. 1997. Resurgent sodium current and action potential formation in dissociated cerebellar Purkinje neurons. *J. Neurosci.* 17:4517–4526.

Raman, I.M., and B.P. Bean. 2001. Inactivation and recovery of sodium currents in cerebellar Purkinje neurons: evidence for two mechanisms. *Biophys. J.* 80:729–737.

Raman, I.M., L.K. Sprunger, M.H. Meisler, and B.P. Bean. 1997. Altered subthreshold sodium currents and disrupted firing patterns in Purkinje neurons of Scn8a mutant mice. *Neuron.* 19:881–891.

Strichartz, G., T. Rando, and G.K. Wang. 1987. An integrated view of the molecular toxinology of sodium channel gating in excitable cells. *Annu. Rev. Neurosci.* 10:237–267.

Tang, L., R.G. Kallen, and R. Horn. 1996. Role of an S4-S5 linker in sodium channel inactivation probed by mutagenesis and a peptide blocker. *J. Gen. Physiol.* 108:89–104.

Tikhonov, D.B., and B.S. Zhorov. 2005. Sodium channel activators: model of binding inside the pore and a possible mechanism of action. *FEBS Lett.* 579:4207–4212.

Ukomadu, C., J. Zhou, F.J. Sigworth, and W.S. Agnew. 1992. μl $Na^+$ channels expressed transiently in human embryonic kidney cells: biochemical and biophysical properties. *Neuron.* 8:663–676.

Wang, S.-Y., and G.K. Wang. 2003. Voltage-gated sodium channels as primary targets of diverse lipid-soluble neurotoxins. *Cell. Signal.* 15:151–159.

Wang, S.-Y., and G.K. Wang. 2005. Block of inactivation-deficient cardiac $Na^+$ channels by acetyl-KIFMK-amide. *Biochem. Biophys. Res. Commun.* 329:780–788.

Wang, S.-Y., K. Bonner, C. Russell, and G.K. Wang. 2003. Tryptophan scanning of D1S6 and D4S6 C-termini in voltage-gated sodium channels. *Biophys. J.* 85:911–920.

West, J.W., D.E. Patton, T. Scheuer, Y. Wang, A.L. Goldin, and W.A. Catterall. 1992. A cluster of hydrophobic amino acid residues required for fast $Na^+$ channel inactivation. *Proc. Natl. Acad. Sci. USA.* 89:10910–10914.

Yeh, J.Z., and T. Narahashi. 1977. Kinetic analysis of pancuronium interaction with sodium channels in squid axon membranes. *J. Gen. Physiol.* 69:293–323.

Yu, F.H., R.E. Westenbroek, I. Silos-Santiago, K.A. McCormick, D. Lawson, P. Ge, H. Ferriera, J. Lilly, P.S. DiStefano, W.A. Catterall, et al. 2003. Sodium channel β4, a new disulfide-linked auxiliary subunit with similarity to β2. *J. Neurosci.* 23:7577–7585.

Zhou, M., J.H. Morals-Cabral, S. Mann, and R. MacKinnon. 2001. Potassium channel receptor site for the inactivation gate and quaternary amine inhibitors. *Nature.* 411:657–661.